Complex-Valued GNN Based Detector for OTFS Signal under Imperfect Channel Information

Yang Yue, *Graduate Student Member, IEEE,* Zan Li, *Fellow, IEEE,* Jia Shi, *Member, IEEE,* Qiang Ni, *Senior Member, IEEE,*

***Abstract*—In recent years, orthogonal time frequency space (OTFS) technique has garnered substantial academic attention as a promising solution for ensuring robust and reliable communication in high-mobility wireless communication environments. In this paper, we present a complex-valued graph neural network (CV-GNN) aided signal detection scheme for OTFS modulation, which can mitigate the channel spreading caused by fractional Doppler shifts. To mitigate inter-carrier interference (ICI) and inter-symbol interference (ISI) induced by fractional Doppler shifts and imperfect channel state information, the proposed detector is able to process the received OTFS signal in the complex plane to acquire the complete phase information of effective channel. Simulation results demonstrate that the proposed method can outperform other state-of-the-art schemes by 1$\sim$4 dB in terms of reliability performance.**

***Index Terms*—Orthogonal time frequency space, signal detection, graph neural network, receiver design.**

I. Introduction

Next-generation wireless communication network will incorporate various high-mobility scenarios, such as unmanned aerial vehicles (UAVs), Internet of Vehicles (IoV), and low-earth-orbit satellites (LEO-Sat), which will suffer severe performance degradation due to fast time-varying channels. However, traditional orthogonal frequency division multiplexing (OFDM) technology is facing significant challenges due to ICI and ISI caused by time-varying channel in high mobility scenes. On the other hand, orthogonal time frequency space (OTFS) [1] technique, a new modulation scheme, has attracted significant attention. OTFS modulation converts a doubly-selective time-frequency (TF) domain channel into an almost time-invariant delay-Doppler (DD) domain channel through a series of two-dimensional (2D) transformations. This undoubtedly provides a new idea to ensure reliable communication in high mobility environments. Each transmitted symbol in the DD domain is spread over the entire TF domain, ensuring that each symbol experiences roughly the same channel gain.

Compared to TF domain, the representation of the channel in DD domain is relatively sparse, which inspires us to design tailored channel estimation and signal detection methods for OTFS to obtain full diversity potential [2], [3]. Motivated by the sparsity of the effective channel matrix in DD domain, a number of compressed sensing (CS) based channel estimation methods have been proposed in the literature [4]–[6]. However, in practical applications, the sparsity of DD domain channel cannot always hold due to the presence of fractional Doppler shifts. The estimation of fractional Doppler faces the following two key challenges: 1) the interference between the pilot and transmitted symbols requires a large guard space; 2) the computational complexity of estimating fractional Doppler shifts is relatively high [7].

In regards to this issue, a number of OTFS channel estimation methods have been proposed in the literature [7]–[13]. Raviteja [7] adopted an embedded pilot based channel estimation method which beneficially arranged the single pilot and data symbols in an OTFS frame. However, when fractional Doppler is present, the 2D transformation of OTFS will diffuse pilot interference throughout the entire frame even with large guard interval, making the channel estimation results inherently prone to errors. To better eliminate the effects of fractional Doppler shifts, the authors in [8] divided grids around integer Doppler values and then proposed a sparse Bayesian learning based methods, which could estimate the DD domain channel response rather than the effective channel matrix. The higher resolution of fractional Doppler partitioning is set, the higher the accuracy of channel estimation can be achieved, while proportionally increasing computational complexity. Since the grids cannot be divided indefinitely, an inherent deviation necessarily exists between the estimated results and true values. Machine learning was also used in [12] where a deep neural network (DNN) was applied to an end-to-end OTFS communication frame directly to avoid channel spreading caused by the fractional Doppler shifts. In the context of grant-free non-orthogonal multiple access OTFS, the authors in [13] significantly enhanced spectral efficiency by substituting guard symbols with training sequences. Additionally, a two-stage channel estimation scheme was designed, which incorporated a parametric approach to refine Doppler estimation, substantially improving estimation accuracy and robustness in high-mobility scenarios.

Due to the low resolution of Doppler frequency shifts, the traditional linear detection methods cannot be directly used in the OTFS frame. Considering the sparsity of DD domain channel, the authors in [14] proposed a message passing (MP) algorithm which models the OTFS frame as a factor graph and approximates the ISI as a Gaussian variable. To improve

This work is supported in part by the National Natural Science Foundation of China (NSFC) (No. 61825104 and No. 62101450) and the National Key R&D Program of China under Grant 2022YFC3301300. (Corresponding author: Jia Shi.)

Yang Yue, Zan Li, Jia Shi are with the School of Telecommunications Engineering, State Key Laboratory of Integrated Service Networks, Xidian University, Xi'an, 710071, China (e-mail: 22011110197@stu.xidian.edu.cn; zanli@xidian.edu.cn; jiashi@xidian.edu.cn).

Qiang Ni is with the InfoLab21, School of Computing and Communications, Lancaster University, U.K (e-mail: q.ni@lancaster.ac.uk).

the convergence performance in the loopy factor graph, a variational Bayes based detector was proposed in [15]. A variety of approximate message passing (AMP) based detection algorithms which can strike a balance between detection performance and computational complexity were proposed in [16]–[20]. The authors in [17] proposed a unitary AMP based OTFS detector which can outperform the MP detector with reduced complexity in the case of rich scattering scenarios. Based on the sparsity of time domain channel, the authors in [19] designed a cross domain iterative detection algorithm, where the estimation and detection approaches were applied in both time domain and DD domain. Nevertheless, the above MP based detection methods assume perfect channel knowledge at the receiver but would suffer severe performance degradation in the presence of channel estimation errors. Although [20] considered the imperfect channel knowledge and designed a model driven DNN method, it can only mitigate interference caused by channel gain error. For OTFS system, the accuracy of estimating channel parameters, especially fractional Doppler shifts, is essential for reconstructing the channel matrix and ensuring reliable signal detection.

Thanks to the efficient ability of exploiting domain features, graph neural network (GNN) has attracted significant attention in solving wireless communication problems [21], especially learning a message passing process [22]–[26]. To further improve the fitting ability of the model, we employed a complex-valued graph neural network (CV-GNN) to improve the performance of GNN based detector. The inputs, weights, and optimization processes in CV-GNN are performed with complex components. These networks exhibit significant advantages in scenarios where the raw data types are in complex value, owing to their ability to preserve phase information in wireless signals and channels [27]–[30]. The contributions of this work are summarized as follows:

1 Motivated by the graph structure of input-output relationship for OTFS modulation scheme, we design a CV-GNN based signal detection method. By converting the detection process to the complex domain, the proposed algorithm is able to utilize phase information of OTFS signals to tackle the channel spreading effect in DD domain, thereby achieving improved error performance.
2 We thoroughly investigate the impact of channel estimation errors on the receiver performance in OTFS systems and demonstrate the robustness of our proposed algorithm against such estimation errors. Moreover, we construct a dataset encompassing both channel gain and Doppler estimation errors, which stimulates to optimize the model with supervised learning. By training the message passing process, the proposed CV-GNN detector can eliminate the inference caused by imperfect channel state information with the capability of retaining the phase information of OTFS signals.
3 We provide the comprehensive performance analysis and the complexity analysis of the proposed detector by comparing other detection methods including maximum likelihood (ML), minimum mean square error (MMSE), orthogonal approximate message passing (OAMP) [18], GNN and graph approximate message passing (AMP-GNN) [24]. Simulation results indicate that the proposed algorithm can significantly outperform the traditional detection algorithms by 4 dB, as well as achieving 2 dB gain over the intelligent algorithms in terms of BER. Meanwhile, the proposed algorithm demonstrates significantly lower runtime compared to other intelligent algorithms, indicating substantial performance gains from the complex-valued network.

Notation: Boldface capitals and lower-case letters are used to define a matrix and a vector, respectively; The superscript T, $*$, and H denote the transpose, conjugate, and the Hermitian operations, respectively; $\mathrm{Tr}[\mathbf{X}]$ denotes the trace of $\mathbf{X}$; $\delta(\cdot)$ denotes the Dirac delta function; $\otimes$ denotes the Kronecker product operator; $\odot$ denotes the element-wise product operator; $\mathrm{diag}\{\cdot\}$ denotes the diagonal matrix; $\mathrm{vec}(\cdot)$ denotes the vectorization operation; $\mathbf{I}$, $\mathbf{0}$, $\mathbf{1}_N$, $\mathbf{F}_N$ denotes the identity matrix, zero matrix, n-dimensional all-ones vector, and N$*$N-dimensional normalized discrete Fourier transform (DFT) matrix. $\Re(\cdot)$ and $\Im(\cdot)$ denote real part and imaginary part; $\mathbb{C}$ denotes the complex domain; $\mathbb{A}$ denotes the modulation alphabet.

II. System model

As shown in Fig. 1, the transmitted OTFS signals in DD domain are denoted by $x[k,l], k = 0,\ldots,N-1, l = 0,\ldots,M-1$, where N and M are the number of samples along the delay and Doppler dimension respectively. It is then mapped to TF domain through the inverse symplectic Fourier transform (ISFFT) operation as [1]

$$X[n,m] = \frac{1}{\sqrt{NM}} \sum_{k=0}^{N-1} \sum_{l=0}^{M-1} x[k,l] e^{j2\pi(\frac{nk}{N} - \frac{ml}{M})}. \quad (1)$$

Assuming the transmit pulse shape $g_{tx}(t)$ and receive pulse shape $g_{rx}(t)$ satisfy bi-orthogonality, $X[n,m]$ can be transformed into a time domain signal $s(t)$ via the Heisenberg transform:

$$s(t) = \sum_{n=0}^{N-1} \sum_{m=0}^{M-1} X[n,m] g_{tx}(t-nT) e^{j2\pi m\Delta f(t-nT)}, \quad (2)$$

where Δf is subcarrier spacing and $T = 1/\Delta f$.

Under the linear time-variant channel, the received signal can be expressed as

$$r(t) = \iint h(\tau,\nu) s(t-\tau) e^{j2\pi\nu(t-\tau)} \mathrm{d}\tau \mathrm{d}\nu + \omega(t). \quad (3)$$

In particular, $h(\tau,\nu)$ denotes the channel impulse response in the DD domain, which can be expressed as

$$h(\tau,\nu) = \sum_{i=1}^{P} h_i \delta(\tau-\tau_i)\delta(\nu-\nu_i). \quad (4)$$

Note that, P denotes the number of paths, h_i, τ_i, and ν_i denote the path gain, delay, and Doppler shift associated with the i-th path, respectively. The delay and Doppler indices are given by

$$\tau_i = \frac{l_i}{M\Delta f}, \qquad \nu_i = \frac{k_i + \kappa_i}{NT}, \quad (5)$$

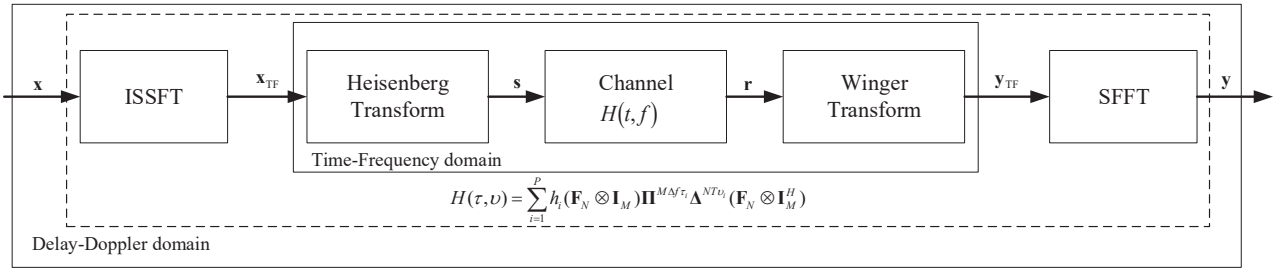

Fig. 1. Flow chart of OTFS signaling.

where l_i and k_i are the delay index and Doppler index of the i-th path. Moreover, $\kappa_i \in [-\frac{1}{2}, \frac{1}{2}]$ is a fractional Doppler associated with the i-th path [14], and $\omega(t)$ denotes the additive white Gaussian noise. For OTFS transmission, $M\Delta f$ is equal to the total bandwidth, and NT is the duration of an OTFS block. Let us assume that, the impact of fractional delays in typical wide band systems can be neglected, due to the sufficiently small value of the delay domain sampling time [14].

Upon applying Winger transform, the received signal from the time domain to the TF domain can be defined as

$$Y(t,f) = \int r(t')g_{rx}^{*}(t'-t)e^{-j2\pi mf(t'-t)}\mathrm{d}t \tag{6}$$

with a receive pulse $g_{rx}(t)$.

The received signal in TF domain can be expressed as follow by sampling at $t = nT$ and $f = \Delta f$:

$$Y[n,m] = Y(t,f)|_{t=nT, f=m\Delta f}. \tag{7}$$

Then the received signal in DD domain can be given by

$$y[k,l] = \frac{1}{\sqrt{NM}} \sum_{n=0}^{N-1}\sum_{m=0}^{M-1} Y[n,m]e^{-j2\pi(\frac{nk}{N}-\frac{ml}{M})} + \widetilde{\omega}[k,l], \tag{8}$$

where $\widetilde{\omega}[k,l]$ denotes the equivalent AWGN samples in DD domain.

The input-output relationship in DD domain can be expressed as

$$y[k,l] \approx \sum_{i=1}^{P}\sum_{q=-N_i}^{N_i}\left(\frac{e^{-j2\pi(-q-\kappa_i)}-1}{Ne^{-j\frac{2\pi}{N}(-q-\kappa_i)}-N}\right)h_i e^{-j2\pi\frac{l_i(k_i+\kappa_i)}{MN}} \times x([k-k_i+q]_N,[l-l_i]_M) + \omega(k,l), \tag{9}$$

where $N_i < N$ if $g_{tx}(t)$ and $g_{rx}(t)$ satisfy the bi-orthogonal property [14]. For each path, the transmitted signal is circularly shifted and scaled by a corresponding channel gain.

We can rewrite (9) in a matrix formula follows:

$$\mathbf{y} = \mathbf{H}_{\mathrm{DD}}\mathbf{x} + \boldsymbol{\omega}. \tag{10}$$

The effective channel matrix in DD domain can be expressed as

$$\mathbf{H}_{\mathrm{DD}} = \sum_{i=1}^{P} h_i(\mathbf{F}_N\otimes\mathbf{I}_M)\mathbf{\Pi}^{l_i}\mathbf{\Delta}^{k_i+\kappa_i}(\mathbf{F}_N^H\otimes\mathbf{I}_M), \tag{11}$$

where $\mathbf{\Pi}$ is the permutation matrix, i.e.

$$\mathbf{\Pi} = \begin{bmatrix} 0 & \cdots & 0 & 1 \\ 1 & \ddots & 0 & 0 \\ \vdots & \ddots & \ddots & \vdots \\ 0 & \cdots & 1 & 0 \end{bmatrix}_{MN\times MN}. \tag{12}$$

Furthermore, $\mathbf{\Delta} = \mathrm{diag}\{\alpha^0, \alpha^1, \cdots, \alpha^{MN-1}\}$ is a diagonal matrix with $\alpha \triangleq e^{\frac{j2\pi}{MN}}$ [31]. Eq. (12) shows the transmitted signal is cyclically shifted according to the delay index l_i and modulated to the carrier frequency with the Doppler index k_i.

As shown in (9), there are $S = \sum_{i=1}^{P}(2N_i+1)$ number of non-zero elements in each row and column of $\mathbf{H}_{\mathrm{DD}}$. Since S is much smaller than NM, the effective channel matrix $\mathbf{H}_{\mathrm{DD}}$ is a sparse matrix. Meanwhile, it can be shown from Eq. (11) that the accuracy of the channel estimation results depends on the estimation for the three parameters, in which the estimation of fractional Doppler is a major challenge to be faced by all channel estimation algorithms.

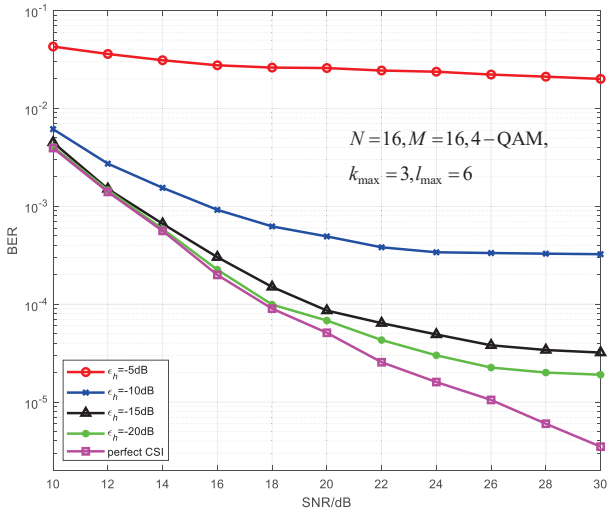

Fig. 2. BER of OAMP detector versus channel estimation error.

In this paper, we consider the presence of channel estimation errors, defining the channel gain and fractional Doppler as [14]:

$$h_i^{'} = h_i + n_{h_i}, \kappa_i^{'} = \kappa_i + n_{\kappa_i}, \tag{13}$$

where $n_h \sim \mathcal{N}(0,\sigma_h^2)$ and $n_\kappa \sim \mathcal{N}(0,\sigma_\kappa^2)$. Additionally, it is assumed that the number of paths, delay and integer

Doppler are perfectly known by the receiver. Fig. 2 illustrates the impact of channel estimation errors on the BER with Eq. (13). It can be observed that when channel estimation errors exist, the error performance of the OAMP detector degrades significantly and exhibits an error floor. Further, the error channel matrix $\widehat{\mathbf{H}}$ can be expressed as

$$\begin{aligned}\widehat{\mathbf{H}} &= \sum_{i=1}^{P}(h_i+n_{h_i})(\mathbf{F}_N\otimes\mathbf{I}_M)\mathbf{\Pi}^{l_i}\mathbf{\Delta}^{k_i+\kappa_i^{'}}(\mathbf{F}_N^H\otimes\mathbf{I}_M)\\ &= \sum_{i=1}^{P}h_i(\mathbf{F}_N\otimes\mathbf{I}_M)\mathbf{\Pi}^{l_i}\mathbf{\Delta}^{k_i+\kappa_i}\cdot\mathbf{\Delta}^{n_{\kappa_i}}(\mathbf{F}_N^H\otimes\mathbf{I}_M)\\ &+ \sum_{i=1}^{P}n_{h_i}(\mathbf{F}_N\otimes\mathbf{I}_M)\mathbf{\Pi}^{l_i}\mathbf{\Delta}^{k_i+\kappa_i}\cdot\mathbf{\Delta}^{n_{\kappa_i}}(\mathbf{F}_N^H\otimes\mathbf{I}_M)\\ &= \mathbf{H}_{\mathrm{DD}}+\mathbf{\Phi}+\mathbf{E}, \end{aligned} \tag{14}$$

where $\mathbf{\Phi} = \sum_{i=1}^{P}h_i(\mathbf{F}_N\otimes\mathbf{I}_M)\mathbf{\Pi}^{l_i}\mathbf{\Delta}^{k_i+\kappa_i}\cdot\mathbf{\Delta}^{n_{\kappa_i}}(\mathbf{F}_N^H\otimes\mathbf{I}_M) - \sum_{i=1}^{P}h_i(\mathbf{F}_N\otimes\mathbf{I}_M)\mathbf{\Pi}^{l_i}\mathbf{\Delta}^{k_i+\kappa_i}(\mathbf{F}_N^H\otimes\mathbf{I}_M)$ and $\mathbf{E} = \sum_{i=1}^{P}n_{h_i}(\mathbf{F}_N\otimes\mathbf{I}_M)\mathbf{\Pi}^{l_i}\mathbf{\Delta}^{k_i+\kappa_i^{'}}(\mathbf{F}_N^H\otimes\mathbf{I}_M)$. Since the error matrix $\mathbf{\Phi}$ is caused by diagonal matrix $\mathbf{\Delta}^{n_{\kappa_i}}$, its structure is similar as $\mathbf{H}_{\mathrm{DD}}$. Therefore, the input-output relationship of OTFS in DD domain can be written by

$$\mathbf{y} = \widehat{\mathbf{H}}\mathbf{x}+\boldsymbol{\omega} = (\mathbf{H}_{\mathrm{DD}}+\mathbf{\Phi}+\mathbf{E})\,\mathbf{x}+\boldsymbol{\omega} = \mathbf{H}_{\mathrm{DD}}\mathbf{x}+\widetilde{\boldsymbol{\omega}}, \tag{15}$$

where $\widetilde{\boldsymbol{\omega}} = \mathbf{\Phi}\mathbf{x}+\mathbf{E}\mathbf{x}+\boldsymbol{\omega}$ is the effective noise vector of OTFS system in the presence of channel estimation error.

According to Eq. (14), the aforementioned assumption indicates that the channel estimation error only affects the values of the elements, but not the structure of the matrix. Therefore, this assumption help preserves the sparsity of the OTFS channel matrix. Motivated by this observation, we propose a GNN based detection algorithm to effectively compensate for channel estimation errors.

III. CV-GNN BASED DETECTOR FOR OTFS

Motivated by the structural characteristics of OTFS transmission matrix and impact of channel estimation errors at the receiver, we propose the CV-GNN detector for the OTFS signal detection. First, we introduce the principles of the GNN module. Subsequently, the network architecture of the proposed CV-GNN based algorithm is presented.

A. Principle of MP based detector

From (10), the joint maximum a posterior probability (MAP) detector for the transmitted signals is given by

$$\hat{\mathbf{x}} = \underset{\mathbf{x}\in\mathbb{A}^{NM\times 1}}{\operatorname{arcmax}}\, P(\mathbf{x}\,|\mathbf{y},\mathbf{H}_{\mathrm{DD}}). \tag{16}$$

Recovering the transmitted signal basing the MAP rule exhibits exponential complexity with respect to MN. The symbol-by-symbol MAP detector for $c = 1,...,NM$ can be expressed as [14]:

$$\begin{aligned}\hat{x}[d] &= \underset{a_j\in\mathbb{A}}{\operatorname{arcmax}}\, P(x[d]=a_j\,|\mathbf{y},\mathbf{H}_{\mathrm{DD}})\\ &\approx \underset{a_j\in\mathbb{A}}{\operatorname{arcmax}}\prod_{c\in J(d)}P(y[c]\,|x[d]=a_j,\mathbf{H}_{\mathrm{DD}}),\end{aligned} \tag{17}$$

where $J(d)$ is the sets of non-zero elements in the c-th column.

The MP based detector, such as expectation propagation, AMP and OAMP, is able to construct a factor graph shown in Fig. 3(a) and iteratively exchanges soft information between factor nodes and variable nodes to build a factorized distribution $q(\mathbf{x})$, which approximates the true posterior distribution $P(\mathbf{x}\,|\mathbf{y},\mathbf{H}_{\mathrm{DD}})$. In order to achieve a trade off between error performance and complexity, the factorized distribution $q(\mathbf{x})$ is approximated by a complex Gaussian distribution, which is characterized by the mean μ and the variance $\mathbf{\Sigma}$. Meanwhile, imperfect channel state information (CSI) significantly affects the accuracy and convergence speed of these algorithms. However, when the channel matrix is ill-conditioned with channel estimation errors, the accuracy of the posterior probability approximation diminishes. Consequently, a number of parameterized detection algorithms have been proposed to effectively maintain both the detection performance and convergence rate [20].

B. GNN based detector framework

Unlike other parameterized detection algorithms, the GNN based approach leverages message passing over a well-defined graph model to iteratively update node feature vectors, effectively capturing both structural and temporal characteristics of the effective channel.

To apply GNN to OTFS detection, it is essential to first model the transmitted signal $\mathbf{x}$ by a pairwise Markov random field (MRF) using an undirected graph $\mathcal{G} = [V, E]$, where the set of nodes V and the set of edges E are defined by $x[c], c = 1,...,NM$ and $\mathbf{H}_{\mathrm{DD}}$, respectively. In a pairwise MRF, the variable node can be characterized by a self potential $\phi(x_i)$, and the (i,j)-th pair of edge is characterized by a pair potential $\phi(x_i,x_j)$. The probability distribution Eq. (16) corresponding to a pairwise MRF is

$$p(\mathbf{x}) = \frac{1}{Z}\prod_{i=1}^{NM}\phi(x_i)\prod_{j\in Ne(i)}\phi(x_i,x_j), \tag{18}$$

where Z is a normalization constant and $Ne(i) = \{x_j\in V\,|\varepsilon_{i,j}\in E\}$. For OTFS signal detection, $\phi(x_i)$ and $\phi(x_i,x_j)$ can be expressed as

$$\phi(x_i) = \exp\left(\frac{1}{\sigma^2}\mathbf{y}^H\mathbf{h}_i x_i - \frac{1}{2}\mathbf{h}_i^H\mathbf{h}_i x_i^2\right)p(x_i), \tag{19}$$

$$\phi(x_i,x_j) = \exp\left(\frac{1}{\sigma^2}\mathbf{h}_i^H\mathbf{h}_j x_i x_j\right), \tag{20}$$

respectively. Within this graph model, each node in the OTFS system is embedded into a feature vector, which is iteratively updated through message aggregation from neighboring nodes. The transmitted signal is then reconstructed via a multi-layer perceptron (MLP).

In order to apply GNN detector to OTFS signals, it is essential to first convert the complex-valued signals to the real domain, given by

$$\mathbf{y}_{\mathrm{r}} = \mathbf{H}_{\mathrm{r}}\mathbf{x}_{\mathrm{r}}+\boldsymbol{\omega}_{\mathrm{r}}, \tag{21}$$

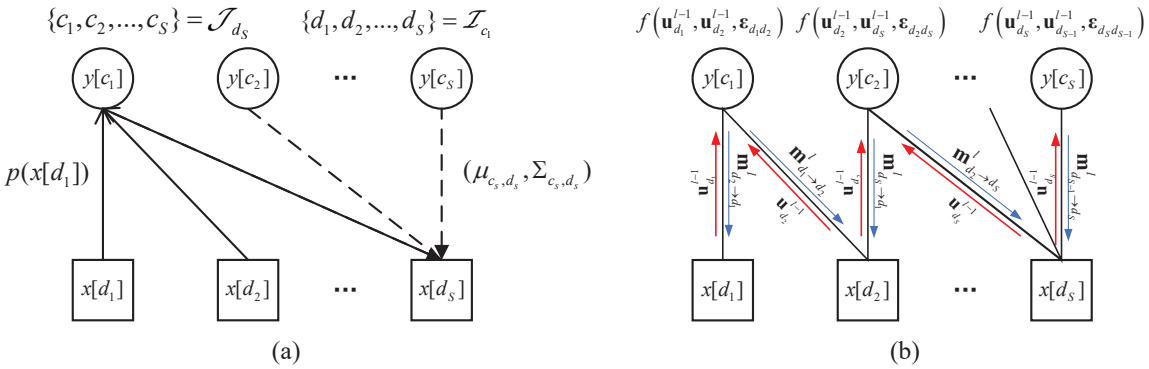

Fig. 3. (a) Factor graph for OTFS detection; (b) GNN detection framework

where $\mathbf{y}_{\mathrm{r}} = \left[\Re\{\mathbf{y}\}^T, \Im\{\mathbf{y}\}^T\right]^T$, $\mathbf{x}_{\mathrm{r}} = \left[\Re\{\mathbf{x}\}^T, \Im\{\mathbf{x}\}^T\right]^T$, $\boldsymbol{\omega}_{\mathrm{r}} = \left[\Re\{\boldsymbol{\omega}\}^T, \Im\{\boldsymbol{\omega}\}^T\right]^T$ and

$$\mathbf{H}_{\mathrm{r}} = \begin{bmatrix} \Re\{\mathbf{H}_{\mathrm{DD}}\}^T & -\Im\{\mathbf{H}_{\mathrm{DD}}\}^T \\ \Im\{\mathbf{H}_{\mathrm{DD}}\}^T & \Re\{\mathbf{H}_{\mathrm{DD}}\}^T \end{bmatrix}. \tag{22}$$

According to Eq. (18), the hidden vector $\mathbf{u}_i^0$ of node i is initialized with

$$\mathbf{u}_i^0 = \mathbf{W}[\mathbf{y}_{\mathrm{r}}^T \mathbf{h}_i, \mathbf{h}_i^T \mathbf{h}_i, \sigma^2]^T + \mathbf{b}. \tag{23}$$

The process of GNN detector can be divided into propagation module, aggregation module and readout module. As shown in Fig. 3(b), in l-th iteration, the propagation module updates message to the variable nodes $\mathbf{m}_{i\to j}^l$ as an encoding of the concatenation of the hidden vectors of nodes i and j and the attributes of the directly connected edge e_{ij}

$$\mathbf{m}_{i\to j}^l = f_{\mathrm{ReLU}}\left(\mathrm{MLP}\left(\mathbf{u}_i^{l-1}, \mathbf{u}_j^{l-1}, \varepsilon_{ij}\right)\right), \tag{24}$$

where $\mathrm{MLP}(\cdot)$ is a MLP and f_{ReLU} is ReLU function.

Then each variable node aggregates the incoming message $\mathbf{m}_{i\to j}^l$ from neighborhood nodes and updates hidden vector by gated recurrent unit (GRU) as following

$$\mathbf{u}_i^l = \mathrm{GRU}\left(\mathbf{u}_i^{l-1}, \sum\nolimits_{j\in Ne_i} \mathbf{m}_{j\to i}^l\right). \tag{25}$$

At the end of the iteration, the hidden vectors of each node $\mathbf{u}_i^K$ are decoded into the marginal probabilities $p(x_i)$ by an MLP with softmax function. The network is optimized by minimizing the cross-entropy loss function

$$\mathrm{loss} = -\sum_{i=1}^{2NM} p(x_i)\log\left(\hat{p}(x_i)\right). \tag{26}$$

As shown in Eq. 15 and Eq. 23, the GNN detector encodes node information into hidden vectors and updates them to approximate the posterior probability of nodes, which inherently contains noise. At the receiver of OTFS systems, channel estimation errors can be modeled as additive noise, thereby allowing adaptation through training. In GNN based algorithms, as the neural networks are incapable of performing complex arithmetic, the real and imaginary parts of the received signal and effective channel matrix in (23) must be explicitly separated and stacked before being input into the neural network. However, the real and imaginary components of communication signals embody critical physical significance, including phase information. Rigid preprocessing of the input signals inevitably leads to a loss of information, thereby limiting the achievable upper bound of detection performance. Therefore, we design a complex-valued graph neural network detector, which differs from the GNN detector discussed in the previous section. In this approach, the feature vectors, network weights, and loss functions are all represented in complex form, making it more aligned with practical OTFS systems.

C. Complex-valued Network Architecture

Our proposed CV-GNN based detector does not directly convert the entire network structure of the GNN detector into complex-valued form, although simulation results demonstrate that such a straightforward adaptation already yields significant performance gains. To further exploit the potential of CV-GNN and enhance the convergence of the neural network, we unfold the iterative algorithm into a neural network, with each layer possessing independent weights rather than sharing weights. The architecture of CV-GNN, as illustrated in the Fig. 4, is composed of multiple residual blocks arranged in series.

1) Initialization: Rather than needing to separate the real and imaginary parts of the inputs in advance, complex value can be fed into the CV-GNN directly. To compute $\mathbf{x}$ through CV-GNN, we denote the N_u-dimensional feature vector of the variable nodes as $\mathbf{u}_i^l$, which is initialized as the concatenation of the received signal, channel state information and noise variance and then encoded by a single layer complex-valued fully connected network (CVFC):

$$\mathbf{u}_i^0 = \mathrm{CVFC}\left([\mathbf{y}^H \mathbf{h}_i, \mathbf{h}_i^H \mathbf{h}_i, \sigma^2]^T\right) = \mathrm{CVFC}\left(\mathbf{u}_{\mathrm{init}}\right), \tag{27}$$

and the CVFC is achieved with two real-valued networks which can be expressed as follows:

$$\begin{aligned} t_1 &= \Re(\mathbf{u}_{\mathrm{init}})\Re(\mathbf{W}) + \Re(\mathbf{b}), \\ t_2 &= \Im(\mathbf{u}_{\mathrm{init}})\Im(\mathbf{W}) + \Im(\mathbf{b}), \\ t_3 &= (\Re(\mathbf{u}_{\mathrm{init}}) + \Im(\mathbf{u}_{\mathrm{init}}))(\Re(\mathbf{W}) + \Im(\mathbf{W})) \\ &\quad + \Re(\mathbf{b}) + \Im(\mathbf{b}). \end{aligned}$$

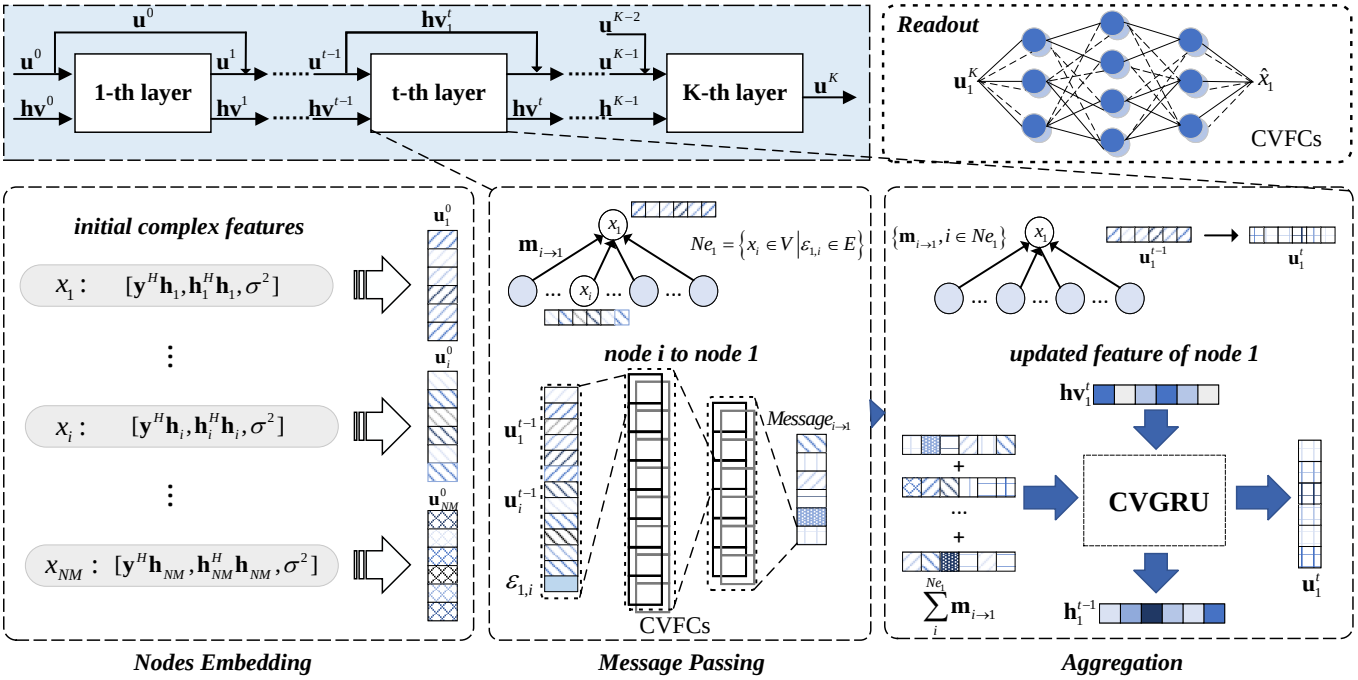

Fig. 4. Network structure of CV-GNN detector

Then the real part and imaginary part of the output $\mathbf{u}_i^l$ can be denoted as

$$\begin{aligned}\Re(\mathbf{u}_i^l) &= t_1 - t_2 \\ &= \Re(\mathbf{u}_{\text{init}})\Re(\mathbf{W}) - \Im(\mathbf{u}_{\text{init}})\Im(\mathbf{W}) + \Re(\mathbf{b}) \end{aligned} \tag{28}$$

$$\begin{aligned}\Im(\mathbf{u}_i^l) &= t_3 - t_2 - t_1 \\ &= (\Re(\mathbf{u}_{\text{init}}) + \Im(\mathbf{u}_{\text{init}}))(\Re(\mathbf{W}) + \Im(\mathbf{W})) \\ &\quad - \Re(\mathbf{u}_{\text{init}})\Re(\mathbf{W}) - \Im(\mathbf{u}_{\text{init}})\Im(\mathbf{W}) + \Im(\mathbf{b}) \\ &= \Im(\mathbf{u}_{\text{init}})\Re(\mathbf{W}) + \Re(\mathbf{u}_{\text{init}})\Im(\mathbf{W}) + \Im(\mathbf{b}), \end{aligned} \tag{29}$$

$$\mathbf{u}_i^l = \Re(\mathbf{u}_i^l) + j\Im(\mathbf{u}_i^l), \tag{30}$$

where $\mathbf{W} \in \mathbb{C}^{3\times N_u}$ and $\mathbf{b} \in \mathbb{C}^{N_u\times 1}$ denote the complex weight and bias parameters.

2) Residual blocks: In the propagation module of l-th residual block, the message from node x_j to x_i can be expressed as

$$\mathbf{m}_{j\to i}^l = f_{\text{CVReLU}}\left(\text{CVFCs}(\mathbf{u}_i^{l-1} + \mathbf{u}_i^{l-2}, \mathbf{u}_j^{l-1} + \mathbf{u}_j^{l-2}, \varepsilon_{ij})\right). \tag{31}$$

The complex split activation function $\text{CVReLU}(\cdot)$ is defined as $\text{ReLU}(\Re(\cdot)) + j\text{ReLU}(\Im(\cdot))$.

Then the aggregated message $\mathbf{m}_i^l = \sum_{j\in Ne_i} \mathbf{m}_{j\to i}^l$ is fed into a complex-valued GRU (CVGRU) as follows

$$\mathbf{hv}_i^l = \text{CVGRU}\left(\mathbf{hv}_i^{l-1}, \mathbf{m}_i^l\right), \tag{32}$$

where $\mathbf{hv}_i^l$ denotes the hidden state of CVGRU. Denoting $\mathbf{W}$ and $\mathbf{U}$ as the weights for $\mathbf{m}$ and $\mathbf{hv}$, the details of the CVGRU is summarized in Appendix A.

Then the node feature will be updated through a single-layer CVFC:

$$\mathbf{u}_i^l = \text{CVFC}\left(\mathbf{hv}_i^l\right). \tag{33}$$

3) Estimation: After obtaining the updated node features at the output layer of the CV-GNN, they are fed into a two-layer CVFCs to directly obtain the value of the data symbol:

$$\hat{x}_i = \text{CVFCs}\left(\mathbf{u}_i^K\right). \tag{34}$$

D. Training Process

In order to optimize complex-valued neural networks, the loss function needs to take into account complex-valued operations. It should be noted that the proposed CV-GNN achieves complex-valued operations through two real-valued networks, thereby requiring the loss to be real-valued. We choose the Split mean-square error (SplitMSE) loss as the cost function, which operates on the real and imaginary parts separately and sums the losses with

$$\begin{aligned}\text{loss} &= \text{SplitMSE}(x_{\text{lable}}, \hat{x}_i) \\ &= \frac{1}{NM}\sum_{i=1}^{NM}\left((\Re(x_{\text{lable}}) - \Re(\hat{x}_i))^2\right. \\ &\quad \left.+(\Im(x_{\text{lable}}) - \Im(\hat{x}_i))^2\right). \end{aligned} \tag{35}$$

To enhance the robustness of the proposed CV-GNN in varying channel conditions, our training dataset incorporates received signals with diverse numbers of paths, channel estimation errors, and noise. The reliability performance of the proposed detector is analyzed in Section IV.

E. Complexity Analysis

We analyze the computational complexity of the CV-GNN and compare it with existing OTFS detectors. The complexity of CV-GNN for one residual block mainly arises

TABLE I
COMPLEXITY OF CV-GNN DETECTOR

Detector	Complexity
CV-GNN	$\mathcal{O}(3MNK\sum_{i=1}^{L}N_{\text{in}}^{i}N_{\text{out}}^{i}+12MNK(2N_o+1)P^2N_u+9MNK(N_hN_u+N_h^2))$
GNN	$\mathcal{O}(2MNK\sum_{i=1}^{L}N_{\text{in}}^{i}N_{\text{out}}^{i}+8MNK(2N_o+1)P^2N_u+6MNK(N_hN_u+N_h^2))$
AMP-GNN	$\mathcal{O}(2MNK\sum_{i=1}^{L}N_{\text{in}}^{i}N_{\text{out}}^{i}+4MNKP^2N_u+6MNK(N_hN_u+N_h^2)+16MN(2N_o+1)P)$

from the CVFCs, which is given by $\mathcal{O}(3MN\sum_{i=1}^{L}N_{\text{in}}^{i}N_{\text{out}}^{i})$. The computational complexity of graph convolution in (31) and (32) is $\mathcal{O}(12MNK(2N_o+1)P^2N_u+9MN(N_hN_u+N_h^2))$, where N_h is the size of hidden layer of CVGRU. Therefore, the computational complexity of CV-GNN detector is $\mathcal{O}(3MN\sum_{i=1}^{L}N_{\text{in}}^{i}N_{\text{out}}^{i}+12MNK(2N_o+1)P^2N_u+9MNK(N_hN_u+N_h^2))$, where K is the number of residual blocks. In contrast, the complexity of GNN and AMP-GNN are $\mathcal{O}(2MNK\sum_{i=1}^{L}N_{\text{in}}^{i}N_{\text{out}}^{i}+8MNK(2N_o+1)P^2N_u+6MNK(N_hN_u+N_h^2))$ and $\mathcal{O}(2MNK\sum_{i=1}^{L}N_{\text{in}}^{i}N_{\text{out}}^{i}+4MNKP^2N_u+6MNK(N_hN_u+N_h^2)+16MN(2N_o+1)P)$ [24].

Compared with other algorithms in Table I, the proposed CV-GNN algorithm incurs higher computational complexity due to complex-valued operations. However, thanks to the performance gains from the complex-valued architecture, the proposed CV-GNN requires significantly lower hidden layer dimensionality than other intelligent detectors, resulting in substantially reduced actual runtime. This will be discussed with comprehensive details in Section IV.

IV. SIMULATION RESULTS

A. System Setting

This section illustrates the BER performance of the proposed CV-GNN detector. An OTFS frame with $N = 8$ and $M = 8$ indicates there are 8 time slots and 8 subcarriers in the TF domain. Assume that the subchannel spacing is $\Delta f = 15$ kHz, and the carrier frequency is $f_c = 4$ GHz. The total number of paths is set as $P = 3$. The velocity of the mobile user is set to be 500 km/h. In this case, the index of delay and Doppler shift can be calculated as $l_{\max} = 3$ and $k_{\max} = 2$, respectively [32], [33]. Especially, the first path always satisfies $l_i = 0$, and the delay index can only be integer-valued while the Doppler index can be fractional. Specially, in order to verify the generalization ability of the trained CV-GNN detector, we generate over 50000 independent data pairs with different SNR ranging from 0 dB to 30 dB to test the network until the number of bit errors exceed 10000.

To demonstrate the performance of our algorithm, we employ several intelligent and non-intelligent algorithms for comparison. It is important to clarify that, to guarantee the fairness of our comparative analysis, extensive parameter optimization is conducted for each GNN-based detector to achieve optimal BER performance under the constraint of an identical network depth. All models are implemented in PyTorch 2.5.1 and trained on a single NVIDIA GeForce RTX 4090 GPU with 24 GB of memory. Training is conducted using the Adam optimizer with an initial learning rate of 1×10^{-3}. A cosine annealing scheduler is employed to decay the learning rate to 1×10^{-5} over 200 epochs. We use a batch size of 50, determined by GPU capacity and to ensure stable gradient estimates. Training is stopped early if the validation loss did not improve for 20 consecutive epochs. Model weights are initialized by sampling from a Gaussian distribution with zero mean and a variance of 0.01.

TABLE II
SYSTEM PARAMETERS

Parameter	Value
Subchannel Spacing (kHz)	15
Carrier Frequency (GHz)	4
Mapping	4-QAM/16-QAM
Number of subcarriers (N)	8
Number of time slots (M)	8
Velocity (km/h)	500
Maximum of the delay index ($l_{\max}$)	3
Maximum of the Doppler index ($k_{\max}$)	2

- **ML** : The optimal detection algorithm performs a global search over all possible transmitted symbol domains by comparing the received signal to each candidate and identifies the transmitted symbol that minimizes the distance to the received signal as the original transmitted symbol.
- **MMSE** : A classical linear receiver which recovers the transmitted signal by applying the noise-regularized pseudo-inverse of the channel matrix to the received signal.
- **OAMP** : An iterative signal recovery algorithm operating by decoupling the estimation process into a linear estimator and a nonlinear denoiser, enforcing an orthogonality principle between their errors to ensure stable convergence and optimal performance [18]. The number of iterations is set to 10.
- **GNN** : The GNN detector given in Section III which is underwentted comprehensive training on the same dataset to ensure fair comparison. The size of the feature vector is set to 16×1 and the size of the hidden vector is set to 512×1.
- **GNN with residual** : The GNN detector with same network structure as CV-GNN which is underwentted

TABLE III
HYPERPARAMETERS OF CV-GNN DETECTOR

Layers	Operation	Number of neurons
Initialized		
Input layer: combined feature with the size of 3×1		
1	CVFC	3×8
Output layer: $\mathbf{u}_i^0$ with the size of 8×1		
Residual block		
Propagation module		
Input layer:concatenated feature with the size of 18×1		
1	CVFC + CVReLU	8×128
2	CVFC + CVReLU	128×64
3	CVFC + CVReLU	64×8
Output layer: $\mathbf{m}_{i\to j}^l$ with the size of 8×1		
Aggregation module		
Input layer: $\mathbf{m}_i^l$ and $\mathbf{hv}_i^{l-1}$ with the size of 8×1 and 128×1		
1	CVGRU	input:8×8, hidden:128×128
2	CVFC	128×8
Output layer: $\mathbf{h}_i^l$ and $\mathbf{u}_i^l$ with the size 128×1 and 8×1		
Estimation module		
Input layer: $\mathbf{u}_i^K$ with the size of 8×1		
1	CVFC	8×128
2	CVFC	128×8
3	CVFC	8×1
Output layer: $\hat{x_i}$ with the size of 1×1		

comprehensive training on the same dataset to ensure fair comparison. The size of the feature vector is set to 16×1 and the size of the hidden vector is set to 256×1.

- **AMP-GNN** : A GNN based detector proposed in [24] which exploits prior information obtained from an AMP module to improve estimates process of a GNN module which is also well trained for fair comparison. The size of the feature vector is set to 16×1 and the size of the hidden vector is set to 512×1.

The hyperparameters of the proposed network are summarized in the Table III.

B. Numerical Results

In Fig. 5, we illustrate the BER performance at different SNR with ideal channel state information and compare the BER performance of the proposed CV-GNN, AMP-GNN [24], GNN, OAMP, MMSE, and ML detector with $P = 3$. We observe that the BER performance improves as the transmit SNR increases. It can be clearly observed that the CV-GNN detector outperforms almost all other OTFS detectors except for ML detector. In particular, the proposed CV-GNN outperforms the AMP-GNN detector by 1 dB and outperforms the GNN detector by 2 dB at $\mathrm{BER} = 1 \times 10^{-4}$, which demonstrates that the complex network of the CV-GNN exhibits enhanced potential for signal detection. The simulation results also indicate that the performance improvement of CV-GNN is not primarily due to the residual structure and deeper networks, although this can help the model converge to the optimal solution more quickly. It is evident from the figure that the proposed CV-GNN algorithm demonstrates significantly superior performance compared to the non-adaptive OAMP and MMSE algorithms. This enhanced performance suggests that CV-GNN is capable of effectively mitigating the impact of Doppler frequency shifts through learned channel characteristics.

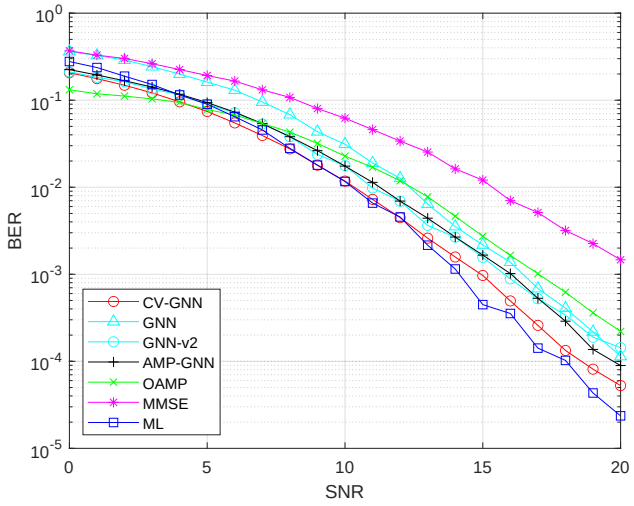

Fig. 5. The BER performance versus SNR with different algorithms.

Additionally, Table IV compares the parameter counts and runtime among different intelligent detectors. It is observed that the proposed detector runs significantly faster than the other detectors, while simultaneously exhibiting a larger parameter size than all intelligent detector except GNN-v2. This demonstrates that, although the proposed CV-GNN trades space complexity for time efficiency, the complex-valued network architecture ultimately contributes to a remarkably enhanced performance.

TABLE IV
PARAMETER COUNTS (M) AND AVERAGE RUNTIME (MS) COMPARISON

Detector	Parameter	Runtime
CV-GNN	1.31	6.81
GNN	0.66	31.19
GNN-v2	6.27	33.72
AMP-GNN	0.68	21.21

Fig. 6 illustrates the BER performance with different paths at $P = 3, 4, 5$ with ideal channel estimation. We observe the BER performance of proposed CV-GNN detector becomes better as the number of paths increases. Although the effective channel matrix in the DD domain $\mathbf{H}_{\mathrm{DD}}$ can be extremely dense at a larger number of the path, the graph based detection procedure and complex computation process can fully harness the diversity gain in DD domain, thus more effectively eliminating interference caused by multipath and fractional Doppler effects.

The BER performance achieved by different OTFS detectors versus the SNR with 4-QAM and 16-QAM in $\mathrm{iter} = 3, 6, 10$ is shown in Fig. 7. We can observe that the proposed algorithm outperforms other GNN based algorithms at all iterations,

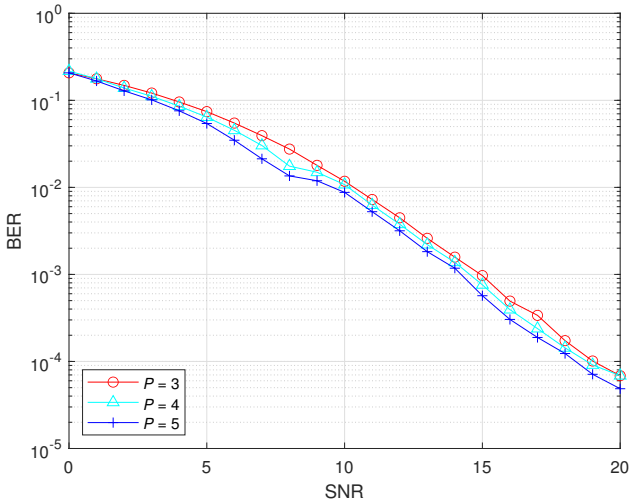

Fig. 6. The BER performance versus SNR with different paths.

which indicates that the complex structure of CV-GNN can make more use of phase information to assist in signal detection. Furthermore, the performance of the CV-GNN algorithm has nearly reached 9×10^{-5} at $\mathrm{SNR} = 20$ dB by the iteration of 6, and at this point, it has already surpassed the performance of AMP-GNN and GNN at 10 iterations, thanks to the deeper neural network. Especially, the BER achieved by proposed CV-GNN detector notably increases with 16-QAM, where the ICI has larger impact to detection accuracy of the GNN based method.

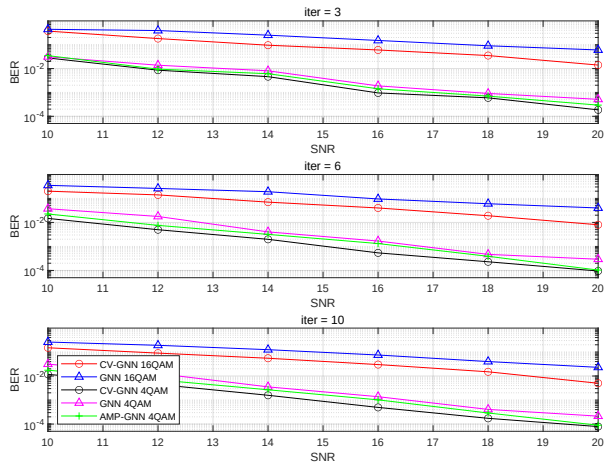

Fig. 7. The BER performance versus SNR with different iteration.

The impact of channel estimation error on the BER performance of the OTFS system is also demonstrated. The error in channel gain and Doppler shift is given by Eq. (13). Fig. 8 shows the BER performance of the CV-GNN, AMP-GNN and MMSE detector with $\sigma_h^2 = 0$ dB, -20 dB, -15 dB, -10 dB and $\sigma_\kappa^2 = 0$ dB, -20 dB, -15 dB at $\mathrm{SNR} = 16$ dB, 20 dB, 24 dB, and 28 dB. We can observe that the imperfect CSI leads to a noticeable degradation in BER performance. As shown in Fig. 8(a) and Fig. 8(b), the detector will encounter error floor during the high-SNR regime due to severe channel estimation errors. Furthermore, estimation errors in channel gain can lead to a more significant degradation in the detection performance. Besides, compared with other algorithms, the proposed CV-GNN detector can achieve lower BER at higher SNR. With $\sigma_h^2 = -15$ dB and $\sigma_\kappa^2 = -15$ dB, the CV-GNN detector can approach 3×10^{-5} at $\mathrm{SNR} = 30$ dB, meanwhile the BER of AMP-GNN and MMSE can only approach 9×10^{-5} and 1×10^{-4}, respectively. This phenomenon is attributed to the enhanced generalization capability brought by the residual module, enabling it to better adapt to the imperfect channel state information.

V. Conclusion

In this paper, we have proposed a complex-valued graph neural network based detector for OTFS transmissions, which conducted the GNN module in the complex domain to fully exploit the phase information of the received signal. The network is designed by expanding the GNN module to residuel blocks and achieving better detection performance by optimizing the parameters through deep learning. Compared with other GNN based detection algorithms, the proposed algorithm demonstrates greater potential in terms of BER performance, owing to its deeper network structure and operations in the complex domain. In the presence of severe ICI caused by fractional Doppler shifts and channel estimation errors in OTFS systems, the proposed algorithm outperforms other algorithms while maintaining acceptable computational complexity. Moreover, the residual network architecture enhances the algorithm's robustness, ensuring stable performance under diverse channel conditions. In future research, we will focus more on the design of efficient and robust detectors for other modulation schemes in the delay-Doppler domain.

Appendix A
Complex-valued GRU

Gated recurrent unit is a variant of recurrent neural network (RNN) designed to address the issues of vanishing and exploding gradients in standard RNN while improving computational efficiency and training speed. In graph neural network, GRU is often applied after the information aggregation process to capture temporal dependencies or sequential patterns in the input data, especially when the graph structure evolves over time.

The input of CVGRU involves the aggregated message $\mathbf{m}^l \in \mathbb{C}^{N_u \times 1}$ and the previous hidden state $\mathbf{hv}^{l-1} \in \mathbb{C}^{N_h \times 1}$, and the flow of information is controlled through the complex update gate $\mathbf{f}_{\text{complex}}^l$ and complex reset gate $\mathbf{r}_{\text{complex}}^l$, achiev-

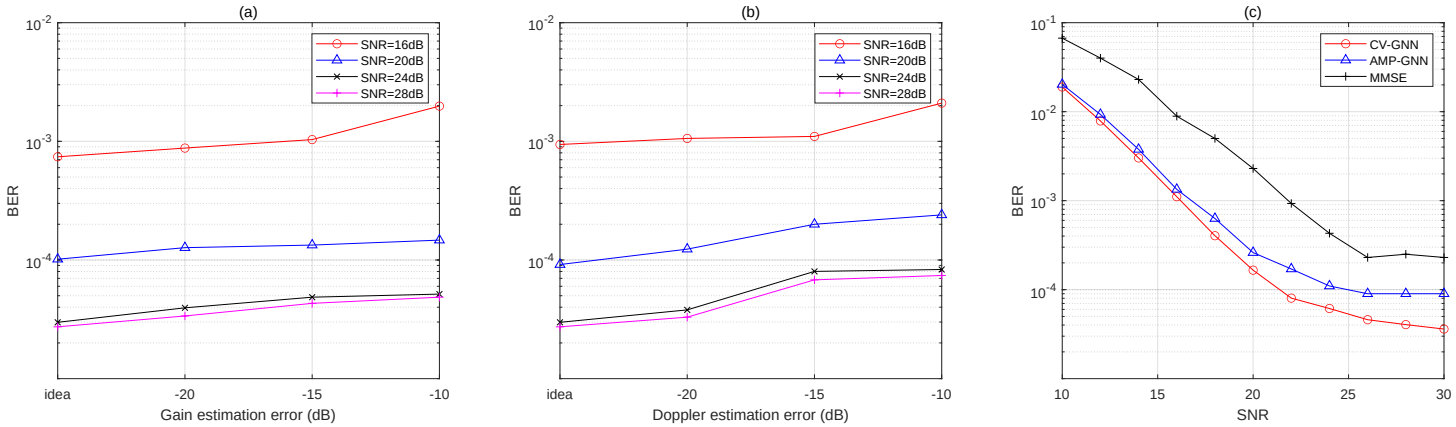

Fig. 8. (a)The BER performance versus SNR with different gain estimation error; (b)The BER performance versus SNR with different Doppler estimation error; (c)The BER performance versus SNR with $\sigma_h^2 = -15$ dB and $\sigma_\kappa^2 = -15$ dB

ing a balance between long-term and short-term memory.

$$\begin{aligned}
&\mathbf{r}^l_{\text{complex}} = \Re\left(\mathbf{r}^l\right) + j\Im\left(\mathbf{r}^l\right), \qquad (36)\\
&\Re\left(\mathbf{r}^l\right) = \sigma\left(\Re\left(\mathbf{m}^l\right)\Re\left(\mathbf{W}^r\right) - \Im\left(\mathbf{m}^l\right)\Im\left(\mathbf{W}^r\right)\right.\\
&\left.+\Re\left(\mathbf{hv}^{l-1}\right)\Re\left(\mathbf{U}^r\right) - \Im\left(\mathbf{hv}^{l-1}\right)\Im\left(\mathbf{U}^r\right) + \Re\left(\mathbf{b}^r\right)\right),\\
&\Im\left(\mathbf{r}^l\right) = \sigma\left(\Re\left(\mathbf{m}^l\right)\Im\left(\mathbf{W}^r\right) + \Im\left(\mathbf{m}^l\right)\Re\left(\mathbf{W}^r\right)\right.\\
&\left.+\Re\left(\mathbf{hv}^{l-1}\right)\Im\left(\mathbf{U}^r\right) + \Im\left(\mathbf{hv}^{l-1}\right)\Re\left(\mathbf{U}^r\right) + \Im\left(\mathbf{b}^r\right)\right),\\
&\mathbf{f}^l_{\text{complex}} = \Re\left(\mathbf{f}^l\right) + j\Im\left(\mathbf{f}^l\right), \qquad (37)\\
&\Re\left(\mathbf{f}^l\right) = \sigma\left(\Re\left(\mathbf{m}^l\right)\Re\left(\mathbf{W}^f\right) - \Im\left(\mathbf{m}^l\right)\Im\left(\mathbf{W}^f\right)\right.\\
&\left.+\Re\left(\mathbf{hv}^{l-1}\right)\Re\left(\mathbf{U}^f\right) - \Im\left(\mathbf{hv}^{l-1}\right)\Im\left(\mathbf{U}^f\right) + \Re\left(\mathbf{b}^f\right)\right),\\
&\Im\left(\mathbf{f}^l\right) = \sigma\left(\Re\left(\mathbf{m}^l\right)\Im\left(\mathbf{W}^f\right) + \Im\left(\mathbf{m}^l\right)\Re\left(\mathbf{W}^f\right)\right.\\
&\left.+\Re\left(\mathbf{hv}^{l-1}\right)\Im\left(\mathbf{U}^f\right) + \Im\left(\mathbf{hv}^{l-1}\right)\Re\left(\mathbf{U}^f\right) + \Im\left(\mathbf{b}^f\right)\right),
\end{aligned}$$

where $\mathbf{W} \in \mathbb{C}^{N_u \times N_h}$, $\mathbf{U} \in \mathbb{C}^{N_h \times N_h}$ and $\mathbf{b} \in \mathbb{C}^{N_h \times 1}$ are learnable parameters. The candidate hidden state is calculated based on the current input $\mathbf{m}^l$ and the reset-modified previous hidden state $\mathbf{hv}^{l-1}$.

$$\begin{aligned}
&\tilde{\mathbf{hv}}^{\,l}_{\text{complex}} = \Re\left(\tilde{\mathbf{hv}}^{\,l}\right) + j\Im\left(\tilde{\mathbf{hv}}^{\,l}\right), \qquad (38)\\
&\Re\left(\tilde{\mathbf{h}}^l\right) = \text{Tanh}\left(\Re\left(\mathbf{m}^l\right)\Re\left(\mathbf{W}^h\right) - \Im\left(\mathbf{m}^l\right)\Im\left(\mathbf{W}^h\right)\right.\\
&+\Re\left(\mathbf{r}^l\right)\odot\left(\Re\left(\mathbf{hv}^{l-1}\right)\Re\left(\mathbf{U}^h\right) - \Im\left(\mathbf{hv}^{l-1}\right)\Im\left(\mathbf{U}^h\right)\right)\\
&\left.+\Re\left(\mathbf{b}^h\right)\right),\\
&\Im\left(\tilde{\mathbf{h}}^l\right) = \text{Tanh}\left(\Re\left(\mathbf{m}^l\right)\Im\left(\mathbf{W}^h\right) + \Im\left(\mathbf{m}^l\right)\Re\left(\mathbf{W}^h\right)\right.\\
&+\Im\left(\mathbf{r}^l\right)\odot\left(\Re\left(\mathbf{hv}^{l-1}\right)\Im\left(\mathbf{U}^h\right) + \Im\left(\mathbf{hv}^{l-1}\right)\Re\left(\mathbf{U}^h\right)\right)\\
&\left.+\Im\left(\mathbf{b}^h\right)\right)
\end{aligned}$$

Combining the candidate hidden state $\tilde{\mathbf{hv}}^{\,l}_{\text{complex}}$ and the previous hidden state $\mathbf{hv}^{l-1}$ using the update gate $\mathbf{f}^l_{\text{complex}}$, the updated hidden state $\mathbf{hv}^l_{\text{complex}}$ is:

$$\begin{aligned}
&\mathbf{hv}^l_{\text{complex}} = \Re\left(\mathbf{hv}^l\right) + j\Im\left(\mathbf{hv}^l\right), \qquad (39)\\
&\Re\left(\mathbf{hv}^l\right) = \Re\left(\tilde{\mathbf{hv}}^{\,l}\right) - \Re\left(\mathbf{f}^l\right)\odot\left(\Re\left(\tilde{\mathbf{hv}}^{\,l}\right) - \Re\left(\mathbf{hv}^{l-1}\right)\right),\\
&\Im\left(\mathbf{hv}^l\right) = \Im\left(\tilde{\mathbf{hv}}^{\,l}\right) - \Im\left(\mathbf{f}^l\right)\odot\left(\Im\left(\tilde{\mathbf{hv}}^{\,l}\right) - \Re\left(\mathbf{hv}^{l-1}\right)\right).
\end{aligned}$$

REFERENCES

[1] R. Hadani, S. Rakib, M. Tsatsanis, A. Monk, A. J. Goldsmith, A. F. Molisch, and R. Calderbank, "Orthogonal time frequency space modulation," in *Proc. IEEE Wireless Commun. Netw. Conf. (WCNC)*, 2017, pp. 1–6.

[2] Z. Wei, W. Yuan, S. Li, J. Yuan, G. Bharatula, R. Hadani, and L. Hanzo, "Orthogonal time-frequency space modulation: A promising next-generation waveform," *IEEE Wireless Commun.*, vol. 28, no. 4, pp. 136–144, Aug. 2021.

[3] J. Shi, Z. Li, J. Hu, Z. Tie, S. Li, W. Liang, and Z. Ding, "OTFS enabled LEO satellite communications: A promising solution to severe doppler effects," *IEEE Network*, vol. 38, no. 1, pp. 203–209, Jan. 2024.

[4] L. Zhao, W.-J. Gao, and W. Guo, "Sparse Bayesian learning of delay-doppler channel for OTFS system," *IEEE Commun. Lett.*, vol. 24, no. 12, pp. 2766–2769, Dec. 2020.

[5] M. Li, S. Zhang, F. Gao, P. Fan, and O. A. Dobre, "A new path division multiple access for the massive MIMO-OTFS networks," *IEEE J. Sel. Areas Commun.*, vol. 39, no. 4, pp. 903–918, Apr. 2021.

[6] W. Shen, L. Dai, J. An, P. Fan, and R. W. Heath, "Channel estimation for orthogonal time frequency space (OTFS) massive MIMO," *IEEE Trans. Signal Process.*, vol. 67, no. 16, pp. 4204–4217, Aug. 2019.

[7] P. Raviteja, K. T. Phan, and Y. Hong, "Embedded pilot-aided channel estimation for OTFS in delay–Doppler channels," *IEEE Trans. Veh. Technol.*, vol. 68, no. 5, pp. 4906–4917, May 2019.

[8] Z. Wei, W. Yuan, S. Li, J. Yuan, and D. W. K. Ng, "Off-grid channel estimation with sparse Bayesian learning for OTFS systems," *IEEE Trans. Wireless Commun.*, vol. 21, no. 9, pp. 7407–7426, Sep. 2022.

[9] I. A. Khan and S. K. Mohammed, "A low-complexity OTFS channel estimation method for fractional delay-Doppler scenarios," *IEEE Wireless Commun. Lett.*, vol. 12, no. 9, pp. 1484–1488, Sep. 2023.

[10] S. P. Muppaneni, S. R. Mattu, and A. Chockalingam, "Channel and radar parameter estimation with fractional delay-Doppler using OTFS," *IEEE Commun. Lett.*, vol. 27, no. 5, pp. 1392–1396, May 2023.

[11] S. R. Mattu and A. Chockalingam, "Learning in time-frequency domain for fractional delay-Doppler channel estimation in OTFS," *IEEE Wireless Commun. Lett.*, vol. 13, no. 5, pp. 1245–1249, May 2024.

[12] L. Guo, P. Gu, J. Zou, G. Liu, and F. Shu, "DNN-based fractional Doppler channel estimation for OTFS modulation," *IEEE Trans. Veh. Technol.*, vol. 72, no. 11, pp. 15 062–15 067, Nov. 2023.

[13] X. Zhou, K. Ying, Z. Gao, Y. Wu, Z. Xiao, S. Chatzinotas, J. Yuan, and B. Ottersten, "Active terminal identification, channel estimation, and signal detection for grant-free NOMA-OTFS in LEO satellite internet-of-things," *IEEE Trans. Wireless Commun.*, vol. 22, no. 4, pp. 2847–2866, Apr. 2023.
[14] P. Raviteja, K. T. Phan, Y. Hong, and E. Viterbo, "Interference cancellation and iterative detection for orthogonal time frequency space modulation," *IEEE Trans. Wireless Commun.*, vol. 17, no. 10, pp. 6501–6515, Oct. 2018.
[15] W. Yuan, Z. Wei, J. Yuan, and D. W. K. Ng, "A simple variational Bayes detector for orthogonal time frequency space (OTFS) modulation," *IEEE Trans. Veh. Technol.*, vol. 69, no. 7, pp. 7976–7980, Jul. 2020.
[16] Y. Ge, Q. Deng, P. C. Ching, and Z. Ding, "Receiver design for OTFS with a fractionally spaced sampling approach," *IEEE Trans. Wireless Commun.*, vol. 20, no. 7, pp. 4072–4086, Jul. 2021.
[17] Z. Yuan, F. Liu, W. Yuan, Q. Guo, Z. Wang, and J. Yuan, "Iterative detection for orthogonal time frequency space modulation with unitary approximate message passing," *IEEE Trans. Wireless Commun.*, vol. 21, no. 2, pp. 714–725, Feb. 2022.
[18] Y. Yue, J. Shi, J. Hu, Z. Tie, and Z. Li, "Performance analysis of oamp detection for orthogonal time frequency space modulation," in *Proc. IEEE ICC Workshop*, May. 2022, pp. 916–921.
[19] S. Li, W. Yuan, Z. Wei, and J. Yuan, "Cross domain iterative detection for orthogonal time frequency space modulation," *IEEE Trans. Wireless Commun.*, vol. 21, no. 4, pp. 2227–2242, Apr. 2022.
[20] Y. Yue, J. Shi, Z. Li, J. Hu, and Z. Tie, "Model-driven deep learning assisted detector for OTFS with channel estimation error," *IEEE Commun. Lett.*, vol. 28, no. 4, pp. 842–846, Apr. 2024.
[21] Y. Shen, J. Zhang, S. H. Song, and K. B. Letaief, "Graph neural networks for wireless communications: From theory to practice," *IEEE Trans. Wireless Commun.*, vol. 22, no. 5, pp. 3554–3569, May 2023.
[22] A. Scotti, N. N. Moghadam, D. Liu, K. Gafvert, and J. Huang, "Graph neural networks for massive MIMO detection," *arXiv preprint arXiv:2007.05703*, Jul. 2020.
[23] H. He, A. Kosasih, X. Yu, J. Zhang, S. Song, W. Hardjawana, and K. B. Letaief, "GNN-enhanced approximate message passing for massive/ultra-massive MIMO detection," in *Proc. IEEE Wireless Commun. Netw. Conf. (WCNC)*, Mar. 2023, pp. 1–6.
[24] W. Zhuang, Y. Mao, H. He, L. Xie, S. Song, Y. Ge, and Z. Ding, "Approximate message passing-enhanced graph neural network for OTFS data detection," *IEEE Wireless Commun. Lett.*, vol. 13, no. 7, pp. 1913–1917, Jul. 2024.
[25] A. Kosasih, V. Onasis, V. Miloslavskaya, W. Hardjawana, V. Andrean, and B. Vucetic, "Graph neural network aided MU-MIMO detectors," *IEEE J. Sel. Areas Commun.*, vol. 40, no. 9, pp. 2540–2555, Sep. 2022.
[26] X. Zhang, S. Zhang, L. Xiao, S. Li, and T. Jiang, "Graph neural network assisted efficient signal detection for OTFS systems," *IEEE Commun. Lett.*, vol. 27, no. 8, pp. 2058–2062, Aug. 2023.
[27] C. Trabelsi, O. Bilaniuk, Y. Zhang, D. Serdyuk, S. Subramanian, J. F. Santos, S. Mehri, N. Rostamzadeh, Y. Bengio, and C. J. Pal, "Deep complex networks," *arXiv preprint arXiv:1705.09792*, May 2017.
[28] J. Bassey, L. Qian, and X. Li, "A survey of complex-valued neural networks," *arXiv preprint arXiv:2101.12249*, Jan. 2021.
[29] J. W. Smith and M. Torlak, "Deep-learning-based multiband signal fusion for 3-d SAR superresolution," *IEEE Trans. Aerosp. Electron. Syst.*, vol. 60, no. 1, pp. 8–24, Jan. 2023.
[30] C. Lee, H. Hasegawa, and S. Gao, "Complex-valued neural networks: A comprehensive survey," *IEEE/CAA J. Autom. Sinica*, vol. 9, no. 8, pp. 1406–1426, Aug. 2022.
[31] P. Raviteja, Y. Hong, E. Viterbo, and E. Biglieri, "Practical pulse-shaping waveforms for reduced-cyclic-prefix OTFS," *IEEE Trans. Veh. Technol.*, vol. 68, no. 1, pp. 957–961, Jan. 2019.
[32] J. Hu, J. Shi, X. Wang, X. Lu, Z. Li, and Z. Tie, "Secrecy transmission of NOMA-OTFS based multicast-unicast streaming," *China Commun.*, vol. 20, no. 1, pp. 1–13, Jan. 2023.
[33] M. Kollengode Ramachandran and A. Chockalingam, "MIMO-OTFS in high-doppler fading channels: Signal detection and channel estimation," in *Proc. IEEE Global Commun. Conf. (GLOBECOM)*, Dec. 2018, pp. 206–212.

Yang Yue (Graduate Student Member, IEEE) received the B.S. degree in communications engineering from Xidian University, Xi'an, China, in 2020. He is currently pursuing the Ph.D. degree with the State Key Laboratory of Integrated Services Networks, Xidian University, Xi'an, China. His research interests include signal detection, channel estimation, and their application in orthogonal time frequency space (OTFS) and affine frequency division multiplexing (AFDM).

Jia Shi (Member, IEEE) received both his MSc. and Ph.D degrees from University of Southampton, UK, in 2010 and 2015, respectively. He was a research associate with Lancaster University, UK, during 2015-2017. Then, he became a research fellow with 5GIC, University of Surrey, UK, from 2017 to 2018. Since 2018, he joined Xidian University, China, and now is a Professor in National Key Lab. of Integrated Services Networks (ISN). His current research interests include resource allocation in wireless systems, covert communications, physical layer security, mmWave communications, satellite communications etc. He is now serving as an Associate Editor for Electronic Letters, and an Editor for International Journal of Communications System, and is serving as a Guest Editor for China Communications.

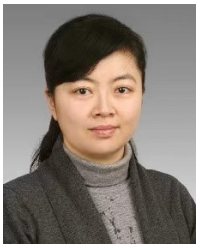

Zan Li (Fellow, IEEE) received the B.S. degree in communications engineering and the M.S. and Ph.D. degrees in communication and information systems from Xidian University, Xian, China, in 1998, 2001, and 2006, respectively. She is currently a Professor with the State Key Laboratory of ISN, School of Telecommunication Engineering, Xidian University. Her research interests include wireless communication and signal processing, particularly covert communication, weak signal detection, spectrum sensing, and cooperative communication. She is a fellow of the Institution of Engineering and Technology (IET), the China Institute of Electronics (CIE), and the China Institute of Communications (CIC). She serves as an Associate Editor for IEEE Transactions on Cognitive Communications and Networking and China Communications.

Qiang Ni (Senior Member, IEEE) is currently a Professor and the Head of the Communication Systems Group, School of Computing and Communications, Lancaster University, Lancaster, U.K. His research interests include the area of future generation communications and networking, including green communications and networking, millimeter-wave wireless communications, cognitive radio network systems, non-orthogonal multiple access (NOMA), heterogeneous networks, 5G and 6G, SDN, cloud networks, energy harvesting, wireless information and power transfer, the Internet of Things (IoT), cyber–physical systems, AI and machine learning, big data analytics, and vehicular networks. He has authored or co-authored more than 300 articles in these areas. He was an IEEE 802.11 Wireless Standard Working Group Voting Member and a contributor to various IEEE wireless standards.